

Optical properties of excitons in CdSe nanoplatelets and disks: real density matrix approach

David Ziemkiewicz,* Gerard Czajkowski, and Sylwia Zielińska-Raczyńska
*Institute of Mathematics and Physics, Technical University of Bydgoszcz,
Al. Prof. S. Kaliskiego 7, 85-789 Bydgoszcz, Poland*

(Dated: June 4, 2024)

We show how to calculate the optical functions of a nanoplatelet, taking into account the effect of a dielectric confinement on excitonic states. Real density matrix approach is employed to obtain analytical and semi-analytical relations for the absorption coefficient, the exciton resonance energy and binding energy of nanoplatelets and nanodisks. The impact of plate geometry (thickness, area) on the spectrum is discussed and the results are compared with the available experimental data.

I. INTRODUCTION

The quantum size effects in semiconductor nanocrystals, first pointed out in 1981 [1] have unlocked plethora of research topics for semiconductor nanosystems [2]. The synthesise of nearly monodisperse semiconductor nanocrystallites, such as cadmium selenide (CdSe) [4] opened the way to producing nanosystems of various dimensions; zero dimensional quantum dots where electrons and holes are confined in three dimensions, one dimensional (1D) nanorods with 2D-confined carriers, and between them are nanoplatelets (NPLs) of a large lateral size but of only a few molecular layers of thickness, with 1D-confined electrons and holes.

Compared with zero-dimensional quantum dots and one-dimensional nanorods, two-dimension nanoplatelets exhibit many unique optical properties. Colloidal two-dimensional semiconductor nanoplatelets, which are atomically flat, exhibit quantum confinement only in one dimension, which results in an electronic structure that is significantly different compared to that of other quantum-confined nanomaterials. The lateral size of these systems can range from a few to tens of nanometers, while in the transverse direction the thickness of NPLs can reach only a few atomic layers, which is smaller than the exciton Bohr radius. The exciton confinement is very strong in the direction perpendicular to the plane of NPLs, but the in-plane motion is free. Cadmium selenide NPLs, first fabricated in 2006 [5] have become important examples of a two-dimensional colloidal nanosystem, with large exciton binding energy, strong quantum confinement and huge oscillator strength, which allows for a high tunability of their optical properties [6]; they exhibit strong and narrow emission lines at both cryogenic and room temperatures [7]. The strong Coulomb interaction leads to exciton binding energy reaching hundreds of meV (the bulk binding energy is only 15 meV); it is remarkable quality of CdSe NPLs, which strongly affects their optical properties.

The light-matter interactions in 2D CdSe NPLs offer several unique advantages in optoelectronic and photonic applications. A high exciton binding energy combined with a specific shape and a confined potential, which limits exciton degrees of freedom in NPLs, lead to a strong exciton-photon interaction in these systems and enables applications of that kind of systems in photonic devices, light-emitting diodes, sensing and light harvesting [2, 3] and references therein. The remarkable thinness of these materials provides unique opportunities for engineering the excitonic properties.

It should be mentioned that nanoplatelets are specific quantum wells (QW), in which electrons and holes are confined in a layer of one type of semiconductors by an impenetrable barrier of a different semiconductor. In the CdSe NPLs considered below the confinement is of electrostatic origin and is caused by a large dielectric mismatch between the semiconductor (here CdSe) and its environment. Despite this difference, electrons and holes interact by a screened Coulomb potential. The bound electron-hole pairs created by a propagating electromagnetic wave are named excitons and they determine the optical properties of the medium. Optical properties of excitons strongly depend on systems size and on shapes of a nanostructure. In a bulk semiconductors excitons resemble hydrogen-like quasiparticles with free center-of-mass motion in all directions, but in quantum dots electrons and holes are confined and so are excitons. As in generic QWs, the optical properties of NPLs are dominated by excitons. So the major part of research on NPLs is concentrated on the calculations of exciton characteristics, such as exciton binding energy, confinement eigenfunctions, and eigenvalues. Recently several groups have measured the exciton binding energy of CdSe NPLs [8–10].

But the sole knowledge of excitonic binding energy is not sufficient to describe, interpret and explain the observed optical spectra. As was pointed by Shornikova *et al.* [9], any approaches which allow one to predict the exciton parameters and their impact on the optical properties are desirable. In the presented work we hope to satisfy this expectation.

The recent growth of interest in such systems encour-

* david.ziemkiewicz@utp.edu.pl

ages us to present a method, which gives a simple analytical expression for optical functions, taking into account confinement and dielectric potentials and any excitonic states, which enables one to obtain theoretical spectra. A majority of authors, describing theoretically the optical properties of excitons in NPLs, are using perturbation calculus, where unperturbed eigenfunctions, describing the carriers motion in the z -direction, are the (finite- or infinite) 1-dimensional quantum well functions. The binding energy is then calculated with Coulomb e-h interaction potential considered as perturbation [11, 12]. A numerical attempt to calculate electronic properties of CdSe NPLs spectra has also been taken by Benchamekh *et al* [8] who applied an advanced tight-binding model. In the present work we propose a different confinement potential, resulting directly from the dielectric confinement. This potential allows for an analytical solution of the Schrödinger equation for electron and hole, describing their motion in the z -(confinement) direction.

We propose a simple confinement potential, which allows an analytical solution of the Schrödinger equation for electron and hole, describing their motion in the z -(confinement) direction. We obtain both eigenfunctions and eigenvalues, which enables to determine the exciton binding energy. Since the solution of the Schrödinger equation for in plane relative motion is well known, we can estimate the total binding energy. Moreover, we present the theoretical method, which allows one to calculate optical properties (i.e., positions of resonances and absorption spectra) of NPLs and nanodisks depending on numbers of monolayers (i.e. thickness of NPLs) . This method called real density matrix approach (RDMA), which takes into account the effects of an anisotropic dispersion and coherence of the electron and the hole with radiation field, allows one to obtain analytical expressions for the susceptibility.

The paper is organized as follows. In Sec. II we recall the basic equations of the used approach (RDMA), adapting them to the case of CdSe NPLs. Sec. III is devoted to specific calculations for nanoplatelets and nanodisks with finite lateral extension. Sec. IV contains theoretical results and comparison with experimental data of the binding energy for systems of different shapes, while in sec. V absorption spectra for NPLs and disks are shown are discussed. The last section presents the concluding remarks.

II. REAL DENSITY MATRIX APPROACH

In this section we briefly review the basic principles of the real density matrix method in the context of linear optical properties of excitons in semiconductors. One of the advantages of RDMA is its formulation in the real space. The method gives a direct relation between the density matrices and the relevant observables, which allows for a straight comparison between experimental and theoretical results. The RDMA has been effectively

applied to the optical excitation spectra of semiconductor bulk crystals, semiconductor superlattices and some low-dimensional structure (see Ref.[13] for a selection of earlier references). After the discovery of the so-called Rydberg excitons, see, for example, Refs.[14, 15] and references therein, RDMA has been successfully applied to describe their optical properties, both linear and nonlinear, see Refs.[16, 17].

The approach starts in the framework of second quantization. The lowest level consists of two-point density matrices, which describe the inter-band transitions between the valence and the conduction band and the intra-band transitions in the indicated bands. Those quantities are important, since there are related to direct measurable quantities as polarization and carrier densities.

The real density matrix approach takes into account the following contributions:

- a) the electron-hole interaction,
- b) the dipole interaction between the electron-hole pairs and the electromagnetic field,
- c) the particle-surface interaction,
- d) effects of external fields.

The basic equations are obtained in the following way. We consider a semiconductor in the real space representation, characterized by a number of valence and conduction bands. Electrons at site j in the conduction band are described by fermion operators $\hat{c}_j^{c\dagger}(\hat{c}_j^c)$ which correspond to creation (annihilation) operators. Similarly, operators $\hat{d}_j^{v\dagger}(\hat{d}_j^v)$ are creation (annihilation) operators for holes in valence bands of a j state. In the case of direct interband transitions Hamilton in our model consists of three parts

$$H = H_0 + H_{em} + H_C. \quad (1)$$

The term H_0 describes one-particle Bloch states in conduction and valence bands and also the intra-band transport processes, the operator H_{em} is an interaction with the electromagnetic field. The physical quantities which are most relevant for the optical properties can be expressed in terms of mean values of the following pair operators

excitonic transition density amplitude

$$Y_{12}^{\alpha b} = \langle \hat{Y}_{12}^{\alpha b} \rangle = \langle \hat{d}_1^\alpha \hat{c}_2^b \rangle,$$

$$\text{electron density } C_{12}^{ab} = \langle \hat{C}_{12}^{ab} \rangle = \langle \hat{c}_1^{a\dagger} \hat{c}_2^b \rangle, \quad (2)$$

$$\text{hole density } D_{12}^{\alpha\beta} = \langle \hat{D}_{12}^{\alpha\beta} \rangle = \langle \hat{d}_1^{\alpha\dagger} \hat{d}_2^\beta \rangle,$$

where the indices $a, b, ..$ and $\alpha, \beta, ...$ stand for conduction and valence bands, respectively. The excitonic transition density $Y_{12}^{\alpha b}$ contributes to the polarization by the following term

$$P = 2 \text{Re} \left(\int_{r=r_1-r_2} d^3r \sum_{cv} M_{21}^{cv*} Y_{12}^{vc} \right), \quad (3)$$

where M_{21}^{cv} is the interband dipole matrix element and the diagonal elements (the matrices C and D) correspond to the densities of electrons

$$\rho_e = -e \sum_c C_{12}^{cc} \Big|_{r_1=r_2}, \quad (4)$$

and holes

$$\rho_h = e \sum_v D_{12}^{vv} \Big|_{r_1=r_2}. \quad (5)$$

These matrices are submatrices of the following density matrix

$$\underline{\hat{\rho}} = \begin{pmatrix} C_{cc'} & Y_{vc}^* \\ Y_{vc} & 1 - D_{vv'} \end{pmatrix}. \quad (6)$$

The dynamics of the two-point functions Y, C, D is part of the hierarchy of reduced density matrices and is obtained from the Heisenberg equations

$$i\hbar \partial_t \underline{\hat{\rho}} = [H, \underline{\hat{\rho}}] + i\hbar \partial_t \underline{\hat{\rho}}_{\text{irrev}}, \quad (7)$$

where the term $\partial_t \underline{\hat{\rho}}_{\text{irrev}}$ describes the dissipation and radiation decay processes, which are due to all dephasing phenomena. In many practical calculations all irreversible processes are described in terms of two dephasing times T_1, T_2 which are taken as phenomenological constants and satisfy the following equation

$$\begin{aligned} \frac{\partial \underline{\hat{\rho}}}{\partial t} \Big|_{\text{irrev}} &= \\ &= - \left(\frac{1}{T_1} [C(t) - C^{(0)}] \frac{1}{T_2} [Y^*(t) - Y^{*(0)}] \right. \\ &\quad \left. - \frac{1}{T_2} [Y(t) - Y^{(0)}] \frac{1}{T_1} [D(t) - D^{(0)}] \right), \end{aligned} \quad (8)$$

where the states with superscript (0) denote the steady state solutions.

Equations (7) then become a closed set of differential equations (usually called constitutive or band-edge equations) for Y, C, D after the following operations [18, 19]:

1. setting up the Heisenberg equations of motion for the pair operators,
2. applying anticommutation rules for the Fermion operators $\hat{c}_j^\dagger, \hat{c}_j^c, \hat{d}_j^{v\dagger}$ and \hat{d}_j^v to bring all operator products into normal order,
3. going over to expectation values,
4. using an interpolation procedure to obtain a continuum dependence on the position variables (for example, Ref.[20]).

As a result we obtain the constitutive equations for interband transition density amplitudes, which for any couple of bands are of the following form

$$\begin{aligned} &-i\hbar \partial_t Y_{12} + H_{eh} Y_{12} \\ &= M_0 (E \delta_{12} - E_1 C_{12} - E_2 D_{21}) - i\hbar \left(\frac{\partial Y_{12}}{\partial t} \right)_{\text{irrev}}. \end{aligned} \quad (9)$$

For intra-band transitions (time dependence of the population of the band states) one has

$$\begin{aligned} &-i\hbar \partial_t C_{12} + H_{ee} C_{12} \\ &= -M_0 (E_1 Y_{12} - E_2 Y_{21}^*) - i\hbar \left(\frac{\partial C_{12}}{\partial t} \right)_{\text{irrev}}, \\ &-i\hbar \partial_t D_{12} + H_{hh} D_{12} \\ &= -M_0 (Y_{21} E_1 - Y_{12}^* E_2) - i\hbar \left(\frac{\partial D_{12}}{\partial t} \right)_{\text{irrev}}. \end{aligned} \quad (10)$$

$$\quad (11)$$

The numerical subscripts are abbreviations for coordinates in the sense $Y_{12} = Y(\mathbf{r}_1, \mathbf{r}_2)$. Hamiltonian H describes propagation in $(\mathbf{r}_1, \mathbf{r}_2)$ space and consists of three parts

$$H = H_{ee} + H_{hh} + H_{eh},$$

which are given by

$$\begin{aligned} H_{eh} &= E_g - V_{12} + \frac{1}{2m_h} (p_1 - eA_1)^2 + \frac{1}{2m_e} (p_2 + eA_2)^2 \\ &+ e (\Phi_1^h - \Phi_2^e), \end{aligned} \quad (12)$$

the electron Hamiltonian

$$H_{ee} = \frac{1}{2m_e} [(p_2 + eA_2)^2 - (p_1 - eA_1)^2] + e (\Phi_1^e - \Phi_2^e), \quad (13)$$

the hole Hamiltonian

$$H_{hh} = \frac{1}{2m_h} [(p_2 - eA_2)^2 - (p_1 + eA_1)^2] - e (\Phi_1^h - \Phi_2^h), \quad (14)$$

where E_g denotes the gap energy, m_e, m_h are the effective masses of electrons and holes, respectively, V_{12} is the statically screened Coulomb potential, M_0 interband transition element integrated over the real space, A_j is the vector potential of the Maxwell field at position \mathbf{r}_j , which may include an external magnetic field, $\Phi_j^{e/h}$ a scalar, external or electromagnetically induced potential acting on electrons (or holes) at position \mathbf{r}_j . E_j denotes the electric field of the radiation at the point \mathbf{r}_j . We neglect for the moment the vectorial and tensorial indices, and use the common notation for the momentum operators: $p_1 = -i\hbar \nabla_1$ etc. The above equations must be solved simultaneously with the Maxwell field equations

$$-c^2 \epsilon_0 \nabla \times \nabla \times \mathbf{E} - \epsilon_0 \epsilon_b \ddot{\mathbf{E}} = \ddot{\mathbf{P}}, \quad (15)$$

where the polarization \mathbf{P} is given by Eq. (3) and ϵ_b is the bulk dielectric constant. When the effects of confinement are considered, one makes use of the appropriate boundary conditions for \mathbf{E}, Y, C and D .

In the weak field limit and for a multiband semiconductor the set of equations (9-11) for the linear case reduces to a set of linearized constitutive equations, which are the inter-band equations (9), where we put $C = D = 0$ on the right-hand side. The resulting equations for the excitonic amplitudes $Y_{12}^{\alpha b}$ of the electron-hole pair of coordinates $\mathbf{r}_1 = \mathbf{r}_h$ and $\mathbf{r}_2 = \mathbf{r}_e$ between any pair of bands α and b have the form

$$-i(\hbar\partial_t + \Gamma_{\alpha b})Y_{12}^{\alpha b} + H_{eh\alpha b}Y_{12}^{\alpha b} = \mathbf{M}_{\alpha b}\mathbf{E}, \quad (16)$$

where $\Gamma_{\alpha b} = \hbar/T_2^{\alpha b}$ is a phenomenological damping coefficient, see Eq. (8). The two-band Hamiltonian $H_{eh\alpha b}$ with energy gap $E_{g\alpha b}$ for any pair of bands reads

$$H_{eh\alpha b} = E_{g\alpha b} + \frac{\mathbf{p}_{h\alpha}^2}{2m_\alpha} + \frac{\mathbf{p}_{eb}^2}{2m_b} + V_{eh}(1, 2) + V_h(1) + V_e(2), \quad (17)$$

with electron and hole kinetic energy operators, m_α and m_b being the band effective masses, V_{eh} describes the electron-hole attraction and V_e, V_h denote the confinement potentials of the electron and the hole, respectively. The total polarization of the medium (3) is related to the excitonic amplitudes by

$$\mathbf{P}(\mathbf{R}) = 2 \sum_{\alpha, \dots, a, \dots} \text{Re} \int d^3r \mathbf{M}_{cv}(\mathbf{r}) Y^{cv}(\mathbf{R}, \mathbf{r}), \quad (18)$$

where $\mathbf{r} = \mathbf{r}_e - \mathbf{r}_h$ is the relative coordinate, and \mathbf{R} the electron-hole pair center-of-mass coordinate, and the summation includes all allowed excitonic transitions between the valence and conduction bands.

III. BASIC EQUATIONS

A. Nanoplatelets

For CdSe based NPLs we have to consider both, heavy(H) and light(L) hole excitons. For the optical transitions between ($\alpha = H, L$) valence bands and the conduction band ($b = C$) we get two constitutive equations for the excitonic amplitudes $Y_{12}^{HC} = Y_H(r_e, r_h)$, $Y_{12}^{LC} = Y_L(r_e, r_h)$

$$\begin{aligned} -i\hbar\partial_t Y_H - i\Gamma_H Y_H + H_{ehH} Y_H &= \mathbf{M}_H(\mathbf{r}) \mathbf{E}(\mathbf{R}), \\ -i\hbar\partial_t Y_L - i\Gamma_L Y_L + H_{ehL} Y_L &= \mathbf{M}_L(\mathbf{r}) \mathbf{E}(\mathbf{R}), \end{aligned} \quad (19)$$

where $\mathbf{M}_{H,L}(\mathbf{r})$ are transition dipole densities. The operators $H_{ehH,L}$ has the form

$$\begin{aligned} H_{ehH,L} &= E_{gH,L} + \frac{p_{ez}^2}{2m_{ez}} + V_e(z_e) \\ &+ \frac{p_{hz}^2}{2m_{hzH,L}} + V_h(z_h) + \frac{\mathbf{p}_{\parallel}^2}{2M_{\parallel H,L}} + \frac{\mathbf{p}_{\parallel}^2}{2\mu_{\parallel H,L}} \\ &+ V_{eh}(z_e - z_h, \rho), \end{aligned} \quad (20)$$

where we have separated the center-of-mass coordinate \mathbf{R}_{\parallel} and the related momentum \mathbf{P}_{\parallel} from the relative coordinate ρ on the plane (x, y) and the related momentum \mathbf{p}_{\parallel} . $M_{\parallel H,L} = m_{h\parallel H,L} + m_{e\parallel}$ is the total in-plane exciton mass. Using Hamiltonian (20) we obtain the constitutive equations in the form

$$\begin{aligned} (H_{ehH} - \hbar\omega - i\Gamma_H)Y_H(\rho, z_e, z_h) \\ = \mathbf{M}_H(\rho, z_e, z_h)\mathbf{E}(\mathbf{R}_{\parallel}, Z). \end{aligned} \quad (21)$$

An analogous equation can be written for the light hole exciton amplitude Y_L .

For a state N we will seek solutions in the form

$$Y_H(\rho, z_e, z_h) = \sum_{j,m,N} c_{jmNH} \psi_{jm}(\rho) \psi_{eN}(z_e) \psi_{hNH}(z_h), \quad (22)$$

where $\psi_{jm}(\rho)$ are the eigenfunctions of the so-called 2-dimensional hydrogen atom, resulting from the equation

$$\left(\frac{\mathbf{p}_{\parallel}^2}{2\mu_{\parallel H}} - \frac{e^2}{4\pi\epsilon_0\epsilon_b\rho} \right) \psi_{jm}(\rho) = E_{jm} \psi_{jm}(\rho), \quad (23)$$

and have the form

$$\begin{aligned} \psi_{jm}(\rho) &= \frac{1}{a_{e\parallel}^*} \frac{e^{im\phi}}{\sqrt{2\pi}} \\ &\times e^{-2\lambda\rho/a_{e\parallel}^*} (4\lambda\rho)^m 4\lambda^{3/2} \frac{1}{(2m)!} \frac{[(j+2m)!]^{1/2}}{[j!]^{1/2}} \\ &\times M(-j, 2|m|+1, 4\lambda\rho) \\ &= R_{jm}(\rho) \frac{e^{im\phi}}{\sqrt{2\pi}}, \\ \lambda &= \frac{1}{1+2(j+|m|)}, \end{aligned} \quad (24)$$

with the confluent hypergeometric function $M(a, b; x)$, defined as an infinite series

$$M(a, b; x) = 1 + \frac{a}{1!b}x + \frac{a(a+1)}{2!(b+1)}x^2 + \dots \quad (25)$$

The eigenvalues, corresponding to the eigenfunctions (24), are given by

$$\frac{E_{jm}}{R_{\parallel}^*} = \varepsilon_{jm} = -\frac{4}{[1+2(j+|m|)]^2}, \quad (26)$$

where R_{\parallel}^* is the Rydberg energy for the in-plane data and $a_{e\parallel}^*$ is the excitonic Bohr radius defined as

$$a_{\parallel,v}^* = \frac{1}{\mu_{\parallel,v}} \epsilon_1 a_B^*, \quad v = H, L. \quad (27)$$

For clarity of the details of subsequent calculations it is sound to mention here that functions $\psi_{e,hN}$ are eigenfunctions of the one-dimensional Schrödinger equations of the type

$$\frac{p_z^2}{2m_z} \psi_{e,hN}(z) + V(z) \psi_{e,hN}(z) = E_z \psi_{e,hN}(z), \quad (28)$$

with a given potential $V(z)$. For further calculations we have to define the form of the confinement potentials $V_{e,h}(z_{e,h})$. The interaction between charged carriers (electrons and holes) with their is described a repulsion potential. In the case of a great mismatch between the dielectric constant of external media ϵ_2 ("out") and the dielectric constant of internal media ϵ_1 ("int") ($\epsilon_2 \ll \epsilon_1$), the "mirror force" is repulsive. This also leads to a repulsive potential that pushes the charge e away from the surface and this force can be described by the repulsive potential, which is inversely proportional to distance from the surface and diverges at least at one of the interfaces. Considering a particle confined in a slab of thickness L , with the surfaces at $z = \pm L/2$, one can solve the Schrödinger equation with a specific one-dimensional model potential, which, with regard to the above description, can be taken in the form

$$V_{e,h}(z) = \frac{\gamma_{e,h}}{(L/2) - z}. \quad (29)$$

The coefficient γ is proportional to dielectric coefficients [21, 22]

$$\gamma \propto \frac{\epsilon_1 - \epsilon_2}{\epsilon_1(\epsilon_1 + \epsilon_2)}.$$

Apart from the confinement potential (29), both carriers (electron and hole) interact also by a Coulomb potential, which leads to the following form of eq. (27)

$$-\frac{\hbar^2}{2m_z} \frac{d^2}{dz^2} \psi_{e,hN}(z) + \frac{\gamma R_z^* a_z^*}{(L/2) - z} \psi_{e,hN}(z) = E_z \psi_{e,hN}(z), \quad (30)$$

where m_z denotes the effective mass of the considered quasi particle (electron or hole) in the z -direction, R_z^* , a_z^* are the corresponding effective Rydberg energies, and Bohr radii defined as

$$R_{e,hz}^* = \frac{m_{e,hz} e^4}{2(4\pi\epsilon_0\epsilon_1)^2 \hbar^2} \quad (31)$$

$$= \left(\frac{m_{e,hz}}{m_0} \right) \frac{1}{\epsilon_1^2} R_B^*,$$

$$a_{e,hz}^* = \frac{\hbar^2(4\pi\epsilon_0\epsilon_1)}{m_{e,hz} e^2} = \left(\frac{m_0}{m_{e,hz}} \right) \epsilon_b a_B^*, \quad (32)$$

where m_0 is the free electron mass, $R_B^* = 13600$ meV and $a_B^* = 0.0529$ nm are the hydrogen Rydberg energy, and Rydberg radius, respectively. The detailed calculations of eigenfunctions and eigenvalues related to Eq. (30) is presented in Appendix A ((A10) and (A16)). They correspond to the lowest excitonic confinement state, so we omit the index N in (22). Making use of the functions (24) and (A16), we calculate the expansion coefficients $c_{jmv,v} = H, L$,

$$c_{jmv} = \frac{\langle M_v^*(\boldsymbol{\rho}, z_e, z_h) | \psi_e(z_e) \psi_h(z_h) \psi_{jmv}(\boldsymbol{\rho}) \rangle}{E_g - \hbar\omega - i\Gamma_v + E_{confv} - E_{bjmv}}, \quad (33)$$

where E_{confv} is given in Eq. (A13), and E_{bjmv} is the so-called binding energy

$$E_{bjmv} = 2 \int_0^\infty \rho d\rho \int_0^{\mathcal{L}_e} d\zeta_e \int_0^{\mathcal{L}_h} d\zeta_h \frac{R_{jm}^2(\rho) \psi_e^2(z_e) \psi_h^2(z_h)}{\sqrt{\rho^2 + (z_e - z_h)^2}}. \quad (34)$$

With the use of the above coefficients we obtain the amplitudes Y_H and Y_L , which determine the NPL polarization by Eq. (18), which in turn enables one to obtain the NPL susceptibility and then, the optical functions.

B. Disks with lateral confinement

It seems that aside from nanoplatelets, nanodisks can also be an important systems in the context of accomplishment and experiments. They are two-dimensional structures of cylindrical symmetry and lateral confinement which may be more suitable for preparation and practical applications. Brumberg *et al.*[12] measured the absorption of CdSe disks. The authors have considered rectangular plates with vertical dimensions typical of the mostly considered CdSe NPLs; systems of such a shape need more complicated theoretical description, which we will be presented below. First, the quadratic shape will be replaced by a cylindrical disk with a radius appropriate to given dimension. The lateral confinement potential for electrons and holes in such a case is given by the expression

$$V_{e,h}(\rho_{e,h}) = \begin{cases} 0 & \text{for } \rho_{e,h} \leq R, \\ \infty & \text{for } \rho_{e,h} > R, \end{cases} \quad (35)$$

Due to the fact that one of the carriers (here the hole) has an effective mass much larger than the other we consider the motion of an electron in the potential (35) supplemented with the Coulomb interaction with the hole, located, in the mean, in the disk center [23]. We will use both negative and positive total energies for the lateral motion.

For the case of negative energies, the respective eigenfunction for the electron motion has the form[23]

$$\psi_{jm}(\xi, \phi) = C \xi^{|m|} e^{-\xi/2} \quad (36)$$

$$\times M \left(m + \frac{1}{2} - \eta, 2|m| + 1; \xi \right) \frac{e^{im\phi}}{\sqrt{2\pi}},$$

where j and m are the principal and magnetic quantum numbers of the excitonic state, $\rho = \rho_e$,

$$\eta = \frac{2}{\kappa}, \quad \xi = \kappa \rho, \quad \kappa^2 = -4 \frac{2m_{e\parallel}}{\hbar^2} a_{e\parallel}^* E = 2/\sqrt{\epsilon}.$$

The quantities κ , ρ , and ξ are dimensionless (defined in the parameters related to the electron). The eigenfunction, due to the no escape boundary condition, satisfies

the equation

$$\psi_{jm}(\alpha\mathcal{R}, \phi) = 0, \quad \mathcal{R} = \frac{R}{a_{e\parallel}^*}, \quad (37)$$

giving the eigenenergies $E_{jm}, m = 0, 1, \dots, j = 0, 1, \dots$. In the linear approximation the first zero will be found from the equation

$$1 + \frac{2m + 2j + 1 - 2\eta_{jm}}{2m + 1} \left(\frac{2}{\eta_{jm}} \mathcal{R} \right) = 0, \quad (38)$$

from which one gets the energy E_{jm}

$$\begin{aligned} \eta_{jm} &= \frac{(2m + 2j + 1)\mathcal{R}}{2\mathcal{R} - 2m - 1} = \frac{2m + 2j + 1}{2} + \nu_{jm}, \\ \nu_{jm} &= \frac{(2m + 2j + 1)(2m + 1)}{2[2\mathcal{R} - 2m - 1]}, \\ E_{jm} &= \frac{1}{\eta_{jm}^2} R_{e\parallel}^*. \end{aligned} \quad (39)$$

Here, we only consider the transverse motion of electron, which does not depend on H-L splitting. Therefore, the index v is omitted in E_{jm} .

With regard to the definitions (39) one can see, that in the limit $\mathcal{R} \rightarrow \infty$ the energies fulfill the expression (26), characterizing the energy of m -states for the so-called 2-dimensional hydrogen atom ($m = 0$ for S -states and $m = 1$ for P -states etc.). From Eqs. (39) we obtain the values of critical radii \mathcal{R}_{cr}

$$\begin{aligned} 2\mathcal{R}_{cr} - 2m - 1 &= 0, \\ \mathcal{R}_{cr} &= \frac{2m + 1}{2}. \end{aligned} \quad (40)$$

Eqs. (39) are applicable for $\mathcal{R} > \mathcal{R}_{cr}$.

In the case of positive energy, the electron eigenfunction has the form[23]

$$\begin{aligned} \psi_{jm}(\rho) &= C e^{-\xi/2} \xi^{|m|} \\ &\times M \left(|m| + \frac{1}{2} - i\eta, 2|m| + 1; \xi \right), \end{aligned} \quad (41)$$

with a normalization constant C . The eigenenergy can be calculated from the condition

$$\text{Re} \psi_{jm}(\mathcal{R}) = 0. \quad (42)$$

With the help of above equations we can express the disk eigenfunctions in a similar way as for NPLs in Sec. III A. We solve the constitutive equations (19), with the Hamiltonian

$$\begin{aligned} H_{ehH} &= E_{gH} + \frac{p_{ez}^2}{2m_{ez}} + V_e(z_e) \\ &+ \frac{p_{hz}^2}{2m_{hzH}} + V_h(z_h) + \frac{\mathbf{P}_{\parallel}^2}{2M_{\parallel H}} + \frac{\mathbf{P}_{\parallel}^2}{2\mu_{\parallel H}} \\ &- \frac{e^2}{4\pi\epsilon_0\epsilon_b\rho_e} + V_e(\rho_e), \end{aligned} \quad (43)$$

where we use the dielectric confinement potentials (29), and $V_e(\rho_e)$ is defined by Eq. (35). Then we look for the solutions in the form (22), using the confinement functions (A16), and the in-plane eigenfunctions $\psi_{jm}(\rho_e)$ (36). The expansion coefficients (33) have now the form

$$c_{jm} = \frac{\langle M(\boldsymbol{\rho}, z_e, z_h) | \psi_e(z_e) \psi_h(z_h) \psi_{jm}(\boldsymbol{\rho}) \rangle}{E_g - \hbar\omega - i\Gamma + E_{confv} - E_{jm}}, \quad (44)$$

where E_{confv} is given in Eq. (A13), and E_{jm} are given in Eq. (39), with appropriate values for the heavy- and light-hole excitons. It should be noted, that these energies contain effects both from the lateral confinement, and the e-h Coulomb interaction.

The next steps are analogous to those described in Sec. II. With such calculated excitonic amplitudes the polarization and then the disk susceptibility can be determined.

IV. CALCULATION OF THE BINDING ENERGY

Since the hole masses (both heavy- and light) are considerably larger than the electron masses, one can neglect the hole contribution in Eq. (34), obtaining

$$|E_{bjmv}| = 2 \int_0^\infty \rho d\rho \int_0^{\mathcal{L}_e} dz_e \frac{R_{jm}^2(\rho) \psi_e^2(z_e)}{\sqrt{\rho^2 + p_v z_e^2}} a_{ez}^* R_{\parallel v}^* \quad (45)$$

where the factor $p_v = \mu_{\parallel v}/m_{ez}$ is due to different scaling of ρ and z_e . With Eq. (45), we obtain the binding energy shown on Fig. 1. For the 1S excitonic state, the

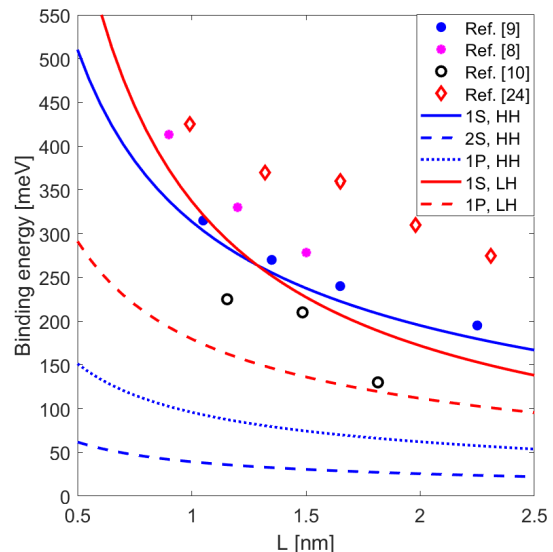


FIG. 1: Comparison of calculated binding energy with literature data [8–10, 24].

heavy hole binding energy is consistent with the data presented in Refs. [8, 9], while different computation models assumed effective masses result in a similar general tendency, but different value of binding energy [8, 24]. Significant differences between various models are discussed in [25]. Our calculations, based on a different confinement potential model, seem to result in a value that is roughly an average of the available literature data. Interestingly, both light- and heavy hole energies are very similar, which results in a significant overlap of these states in the absorption spectrum, as will be shown later. The $1P$ state energies are considerably smaller. Note that the binding energy is strongly dependent on the effective masses; for the details of their fits to the available literature data, see Appendix B.

In the case of nanodisks, one can estimate the binding energy as a function of the disk area. The energies (39) contain contributions from both the confinement energy and the binding energy. To extract the binding energy, we can use the perturbation calculus. The unperturbed eigenfunctions are the solutions of Eq. (45) and have the form

$$\psi_{nm}(\rho) = N_{mn} J_m \left(\frac{\rho}{\mathcal{R}} j_{mn} \right), \quad (46)$$

where N_{mn} are the corresponding normalization factors, and j_{mn} the zeros of the Bessel functions J_m , \mathcal{R} is defined in Eq. (37). With the eigenfunctions (46), we can apply the formula (45), where now

$$|E_{bmn}| = 2 \int_0^{\mathcal{R}} \int_0^{\mathcal{L}_e} \rho d\rho dz_e \frac{\psi_{mn}^2(\rho) \psi_e^2(z_e)}{\sqrt{\rho^2 + p_e^2 z_e^2}} a_{ez}^* R_{||e}^*, \quad (47)$$

where

$$p_e = \frac{m_{e||}}{m_{ez}}, \quad R_{||e}^* = \frac{m_{e||} R_B^*}{\epsilon_1^2}, \quad (48)$$

The binding energies calculated with Eq. (46) are shown on Fig. 2. Our calculations result in a fairly good match to the data in Ref. [12], correctly predicting the general tendencies and confirming that modeling a square plate as a disk is a valid approximation. Interestingly, even for non-square plates the model works fairly well. Again, it should be stressed that the results depend heavily on the assumed model of the effective masses.

As a next step, we can calculate the energy of S and P excitons to estimate the S-P splitting. A comparison of the calculated splitting with the experimental data from [9] and model from [11] is shown on Fig. 3. We get an excellent agreement with available measurements [9, 11].

V. CALCULATION OF ABSORPTION SPECTRUM

In the considered NPLs widths the typical wavelength of the input electromagnetic wave is much larger than

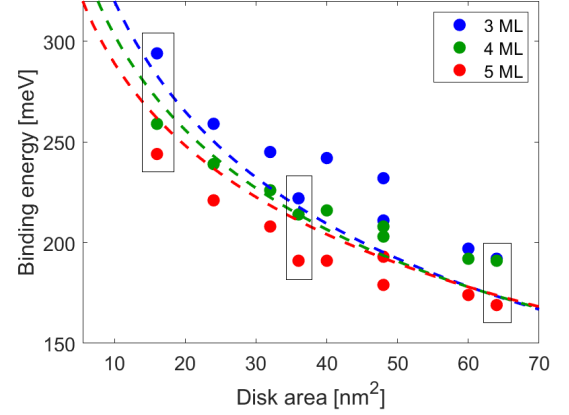


FIG. 2: Comparison of calculated binding energy with [12]. Boxes mark the data for square platelets.

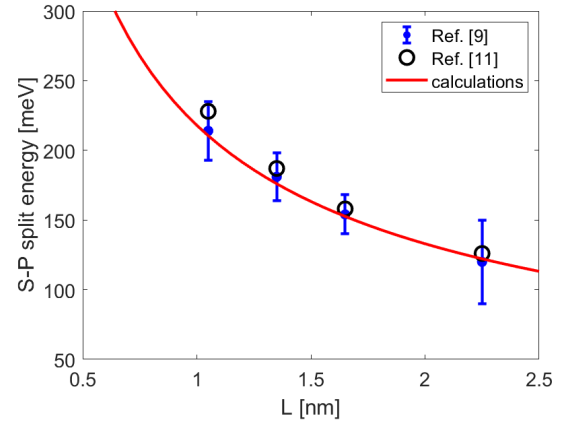


FIG. 3: Comparison of calculated S-P splitting energy with Refs. [9, 11]

the NPLs width, so we can use the long wave approximation. For further calculations we need to define the dipole density function \mathbf{M} . The transition dipole density $M(\rho)$ should have the same symmetry properties as the solution of the corresponding Schrödinger equation. Therefore, in the case of 2-dimensional systems, we apply the dipole density $M_m(\rho, \phi)$ in the form

$$\begin{aligned} M_{mv}(\rho, \phi; z_e, z_h) &= \\ &= \frac{M_{0mv} \rho^m}{(m+1)! \rho_{0v}^{m+2}} e^{-\rho/\rho_{0v}} \frac{e^{im\phi}}{\sqrt{2\pi}} \delta(z_e - z_h), \end{aligned} \quad (49)$$

where $\rho_{0v} = r_{0v}/a_{||v}^*$ are the so-called coherence radii, defined as

$$\rho_{0v} = \sqrt{\frac{R_{||v}^*}{E_{gv}}}. \quad (50)$$

The above equation also indicates, that the integrated dipole strength M_{0mv} and its relation to the longitudinal-transversal energy will depend on the quantum number

m . Since we will consider both S and P excitons, the expressions for $m = 0$ and $m = 1$ have to be used. The dipole matrix elements for $m = 0$ have the form [13]

$$\begin{aligned} M_{00H}^2 &= \frac{\pi}{2} \epsilon_0 \epsilon_b a^*{}^3 \Delta_{LT}, \\ M_{00L}^2 &= \frac{1}{3} M_{00H}^2. \end{aligned} \quad (51)$$

For $m = 1$ the coefficient M_{01H} and the coherence radius r_{0H} are related to each other by the longitudinal-transversal energy Δ_{LT} described by the following relation [23]

$$\begin{aligned} (M_{01H} \rho_{0H})^2 &= \frac{4}{3} \frac{\hbar^2}{2\mu_{\parallel H}} \epsilon_0 \epsilon_b a^* \frac{\Delta_{LT}}{R_H^*} e^{-4\rho_{0H}} \\ &= \frac{4}{3} \epsilon_0 \epsilon_b a^*{}^3 \Delta_{LT}, \end{aligned} \quad (52)$$

a^* being the bulk exciton radius. With the above definitions we have all elements to calculate the mean NPL susceptibility. For the normal incidence both the electric field of the wave propagating in the NPL and the polarization (18) depend on the center-of-mass coordinate Z . The mean NPL susceptibility can be written in the form

$$\bar{\chi} = \frac{1}{L} \int_{-L/2}^{L/2} \frac{P(Z)}{\epsilon_0 E(Z)} dz. \quad (53)$$

Making use of the equations (22), (18), (51), (52), and taking into account the relevant resonances, we obtain the susceptibility of the considered CdSe NPL

$$\begin{aligned} \bar{\chi}(\omega, L) &= A_{ehH} \epsilon_1 \Delta_{LT} \left(\frac{\mu_{\parallel H}}{\mu_{\parallel bulk}} \right)^2 \left[\frac{\chi'_{00H}}{E_{res}(1SH) - \hbar\omega - i\Gamma_H} \right. \\ &+ \frac{\chi'_{10H}}{E_{res}(2SH) - \hbar\omega - i\Gamma_H} + \frac{\chi'_{01H}}{E_{res}(1PH) - \hbar\omega - i\Gamma_H} \\ &+ \frac{1}{3} A_{ehL} \epsilon_1 \Delta_{LT} \left(\frac{\mu_{\parallel L}}{\mu_{\parallel bulk}} \right)^2 \\ &\times \left[\frac{\chi'_{00L}}{E_{res}(1SL) - \hbar\omega - i\Gamma_L} + \frac{\chi'_{01L}}{E_{res}(1PL) - \hbar\omega - i\Gamma_L} \right], \end{aligned} \quad (54)$$

where

$$\begin{aligned} \chi'_{00H} &= \pi \frac{16}{(1 + 2\rho_{0H})^4}, \\ \chi'_{100} &= 0.6 \pi \left(\frac{3}{3 + 2\rho_{0H}} \right)^6 (1 - 2\rho_0)^2, \\ \chi'_{01H} &= 1.6 \left(\frac{3}{3 + 2\rho_{0H}} \right)^6, \\ \chi'_{00L} &= \pi \frac{16}{(1 + 2\rho_{0L})^4}, \\ \chi'_{01L} &= 1.6 \left(\frac{3}{3 + 2\rho_{0L}} \right)^6. \end{aligned} \quad (55)$$

The quantities A_{ehv} are related to the overlap integrals

$$\begin{aligned} A_{ehv} &= \frac{a^*}{L} |\langle \psi_e(z_e) \delta(z_e - z_h) \psi_{hv}(z_h) \rangle|^2 \\ &= \left(\frac{a_{bulk}^*}{L} \right) a_{ez}^* a_{hzv}^*. \end{aligned} \quad (56)$$

The quantities A_{ehv} determine the relation between the maxima of the heavy-hole and light-hole resonances

$$\begin{aligned} \frac{\max H}{\max L} &= 3 \frac{A_{ehH} \Gamma_L}{A_{ehL} \Gamma_H} \left(\frac{\mu_{\parallel H}}{\mu_{\parallel L}} \right)^2 \left(\frac{1 + 2\rho_{0L}}{1 + 2\rho_{0H}} \right)^4 \frac{m_{hzL}}{m_{hzH}} \\ &= 3 \frac{\Gamma_L}{\Gamma_H} \left(\frac{\mu_{\parallel H}}{\mu_{\parallel L}} \right)^2 \left(\frac{1 + 2\rho_{0L}}{1 + 2\rho_{0H}} \right)^4 \frac{\gamma_1 - 2\gamma_2}{\gamma_1 + 2\gamma_2}. \end{aligned} \quad (57)$$

The calculated absorption coefficient $A = 1 - R - T$ is shown on Fig. 4. We obtain an excellent agreement

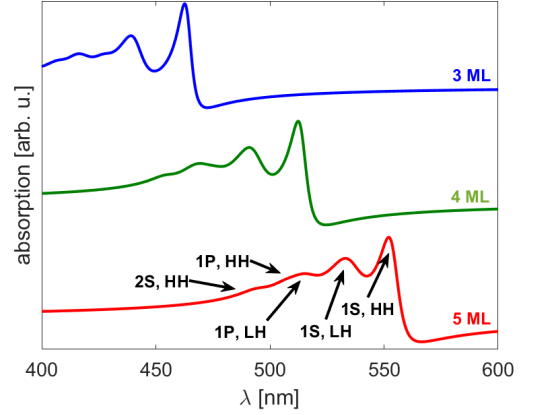


FIG. 4: Calculated absorption spectra for 3,4,5 monolayers platelet. Individual excitonic states are indicated by arrows.

with measured spectra in literature [2, 9–12, 24, 27]. The calculated binding energies and resonance energies corresponding to individual peaks in the absorption spectrum are summarized in Table I. For a particular example, for $L = 4$ monolayers, $1S$ heavy hole peak is located at 2410 meV, which corresponds to $\lambda = 514$ nm. In comparison, the measured peak positions for this thickness are 513 nm [12], 493 nm [9], 512 nm [2, 24]. The dominant feature of the spectrum are two main peaks corresponding to heavy- and light hole $1S$ exciton, located approximately 30-40 nm apart, consistently with Refs. [9–12, 27]. The light hole peak is usually wider and in some experiments, it seems to have a complex structure [10]. We can attribute this to an overlap of several weaker maxima corresponding to $1P$ and $2S$ states of light and heavy holes (see arrows on Fig. 4). To further clarify the structure of the spectrum, Fig. 5 depicts the individual contributions of light and heavy hole excitons to the spectrum of 5 monolayer platelet. Noticeably, $1P$ states of light and heavy holes overlap almost completely, making them impossible to distinguish in the total spectrum. Note that the

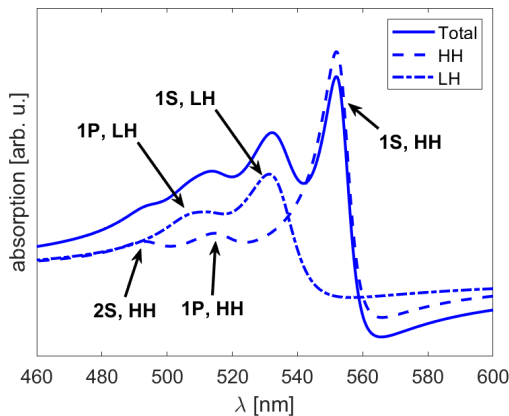


FIG. 5: Calculated absorption spectra for 5 monolayers platelet, divided into light- and heavy hole contribution. Individual excitonic states are indicated by arrows.

linewidths Γ_v of individual state absorption lines were fitted to match the experimental spectra, in particular [10], where some of the fine features of the spectrum discussed here can be seen in the measurements.

The absorption spectrum of a disk is also calculated from Eq. (54), but with the appropriate resonance energies given by denominator of Eq. (44). The results are shown on Fig. 6. In the limit of large area, the peaks

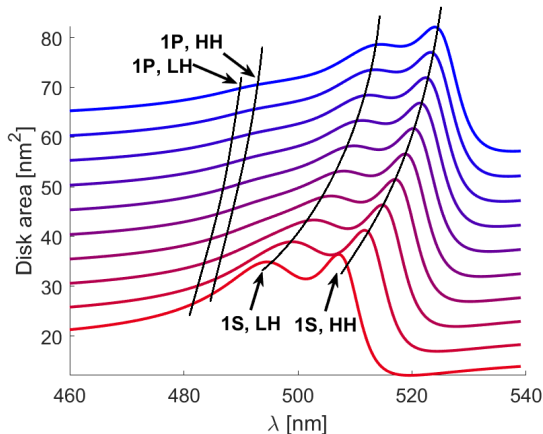


FIG. 6: Calculated absorption spectra for 4 monolayer disks with various areas. Individual excitonic states are indicated by arrows.

of absorption spectrum asymptotically approach the energies measured by [12], where square plates with area on the order of 100 nm^2 were considered. In general, the wavelength of exciton peaks increases with the disk area, with the largest change occurring for $1S$ state.

| Parameter | 3ML | 4ML | 5ML |
|-------------------|--------|--------|--------|
| L | 1 | 1.33 | 1.67 |
| $E_b(1SH)$ | 313.75 | 258.00 | 220.82 |
| $E_b(2SH)$ | 39.22 | 32.86 | 28.57 |
| $E_b(1PH)$ | 95.80 | 80.11 | 69.54 |
| $E_b(1SL)$ | 336.88 | 255.48 | 204.86 |
| $E_b(1PL)$ | 179.57 | 147.80 | 126.54 |
| $E_{conf,H}$ | 1170 | 839 | 667 |
| $E_{conf,L}$ | 1528 | 1060 | 819 |
| $E_{res}(1SH)$ | 2670 | 2410 | 2237 |
| $E_{res}(2SH)$ | 2954 | 2649 | 2439 |
| $E_{res}(1PH)$ | 2896 | 2599 | 2396 |
| $E_{res}(1SL)$ | 2808 | 2511 | 2312 |
| $E_{res}(1PL)$ | 2974 | 2632 | 2399 |
| $S - P$ split | 218 | 178 | 153 |
| $S - P$ split [9] | 214 | 181 | 154 |

TABLE I: Binding energies and resonance energies of a platelet [meV], electron mass from [8]

VI. CONCLUSIONS

In this paper we have discussed some remarkable optical properties of CdSe monolayers systems. Atomically thin CdSe NPLs have unique physical properties which could be valuable for a broad range of applications [2], [28]. Strong light-matter interaction and atomically thin volume are advantages for 2D semiconductors which make them easy tunable, as the optical properties can be controlled using multiple modulation methods. The remarkable thinness of these materials also provides unique opportunities for engineering the excitonic properties. For example, changing the dielectric environment of NPLs significantly reduces the exciton binding energies and the free-particle band gap. With the help of RDMA, using dielectric potential resulting from the dielectric confinement, we have derived analytical expressions for the binding energy and absorption for systems of NPLs and disks depending on the monolayers number. Our results have been thoroughly discussed and compared with the available experimental data showing a fairly good agreement. This approach and results may open up a variety of possibilities to manipulate excitonic states on the nanometer scale in 2D materials in the future.

Appendix A: Eigenfunctions of the dielectric confinement

We consider the equation

$$-\frac{\hbar^2}{2m_z} \frac{d^2}{dz^2} \psi(z) + \frac{\gamma R_z^* a_z^*}{(L/2) - z} \psi(z) = E_z \psi(z), \quad (\text{A1})$$

Using the relation

$$\frac{2m_z}{\hbar^2} = \frac{1}{R_z^* a_z^{*2}}, \quad (\text{A2})$$

where m_z, R_z^*, a_z^* are taken for a given quasi particle, and denoting,

$$\begin{aligned} \ell &= \frac{L}{2a_z^*}, \quad \zeta = \frac{\ell - z}{a_z^*}, \\ \varepsilon &= \frac{E}{R^*}, \quad \kappa = 2\sqrt{\varepsilon}, \quad z' = -i\kappa\zeta, \end{aligned} \quad (\text{A3})$$

we transform the Eq. (A1) into the form

$$\frac{d^2\psi}{dz'^2} + \left[-\frac{1}{4} + \frac{\lambda}{z'} + \frac{\mu^2 - 1/4}{z'^2} \right] \psi = 0, \quad (\text{A4})$$

where

$$\lambda = -\frac{i\gamma}{\kappa}, \quad \mu = \frac{1}{2}.$$

The equation (A4) has the form of a Whittaker equation. The solutions of (A4) are the Whittaker functions (see, for example, [26]) $M_{\lambda,\mu}(x), W_{\lambda,\mu}(x)$; we use the first one in the form

$$\begin{aligned} M_{\lambda,\mu}(z') &= \\ &= x^{\mu+1/2} e^{-z'/2} M\left(\mu - \lambda + \frac{1}{2}, 2\mu + 1; z'\right), \end{aligned} \quad (\text{A5})$$

with the confluent hypergeometric function $M(a, b; x)$.

Substituting $\mu = 1/2$ we obtain the solution of Eq. (30) in the form

$$\psi(z') = C z' e^{-z'/2} M(1 - \lambda, 2; z'), \quad (\text{A6})$$

with the normalization constant C .

The confinement condition requires vanishing of the eigenfunction on the platelet interfaces. The condition $\psi(z = L/2) = 0$ is automatically satisfied, as follows from the formula (A6). The condition $\psi(z = -L/2) = 0$, which can be written in the form

$$\psi(-i\kappa\ell) = 0, \quad (\text{A7})$$

will be used to calculate the confinement states energies.

As it follows from Eq. (18), only the real part of the function Y contributes. Therefore we solve the Eq. (A7) by putting

$$\text{Re} M\left(1 + \frac{i\gamma}{\kappa}, 2; -i\kappa\ell\right) = 0. \quad (\text{A8})$$

Taking the lowest terms from the expansion (25) and leaving the terms linear in γ , we obtain the relation

$$1 + \frac{\gamma\ell}{2} - \frac{1}{6}\kappa^2\ell^2 = 0. \quad (\text{A9})$$

Using the definitions of κ and ℓ , we arrive at the eigenenergies of the dielectric confinement

$$E_{e,hz} = \frac{6\beta[1 + (\gamma_{e,h}\ell_{e,h}/2)]}{m_{e,hz}L^2}, \quad (\text{A10})$$

which give the total confinement energy

$$\begin{aligned} E_{conf} &= E_{ez} + E_{hz} \\ &= \frac{1}{\mu_z} \frac{6\beta}{L^2} + \frac{3\beta\gamma_e \ell_e}{m_{ez}L^2} + \frac{3\beta\gamma_h \ell_h}{m_{hz}L^2}, \end{aligned} \quad (\text{A11})$$

with β

$$\beta = a_B^{*2} \times R_B^* = 38 \text{ nm}^2 \text{ meV}, \quad (\text{A12})$$

where $[L] = \text{nm}$. Using the value of β , and the definitions

$$\ell_{e,h} = \frac{L}{2a_{ze,h}^*}, \quad a_{ze,h}^* = \frac{1}{m_{ze,h}} \epsilon_b a_B^*,$$

we obtain the confinement energy

$$\begin{aligned} E_{confv}(L) &= \frac{1}{\mu_{zv}L^2} 228[\text{nm}^2 \text{ meV}] \\ &+ \frac{\gamma}{L} 359[\text{nm meV}], \end{aligned} \quad (\text{A13})$$

where

$$\gamma = \gamma_e + \gamma_h, \quad v = H, L \quad (\text{A14})$$

with E given in meV and L in nm. The factor 359 is obtained from the relation

$$\frac{3\beta}{L} \left(\frac{\ell_e}{m_{ez}} + \frac{\ell_h}{m_{hz}} \right) = \frac{3\beta}{\epsilon_1 a_B^*}, \quad (\text{A15})$$

when using $\epsilon_1 = 6$.

Using Eq. (A6), where we take the lowest three terms and (A9), we obtain the normalized eigenfunctions for the dielectric confinement in the form

$$\begin{aligned} \psi_{e,h}(z_{e,h}) &= C(-i\kappa_{e,h}z_{e,h}) \exp\left[\left(\frac{i\kappa_{e,h}z_{e,h}}{2}\right)\right] \\ &\times \text{Re} \left[M\left(1 + \frac{i\gamma}{\kappa}, 2; -i\kappa z_{e,h}\right) \right] \\ &= C(-i\kappa_{e,h}z_{e,h}) \exp\left[\left(\frac{i\kappa_{e,h}z_{e,h}}{2}\right)\right] \\ &\times \sqrt{\frac{13.12}{\mathcal{L}_{e,h}}} \frac{\zeta_{e,h}}{\mathcal{L}_{e,h}} \left(1 - \frac{\zeta_{e,h}^2}{\mathcal{L}_{e,h}^2}\right), \end{aligned} \quad (\text{A16})$$

where

$$\zeta_{e,h} = \frac{z_{e,h}}{a_{e,hzv}^*}, \quad \mathcal{L}_{e,hv} = \frac{L}{a_{e,hzv}^*}.$$

Appendix B: Estimation of effective masses

There are several literature sources regarding the electron effective mass in CdSe nanoplatelets. One set of masses, obtained in [9] from numerical calculations, can be described with exponential fits

$$\begin{aligned} m_{ez} &= 0.12 + 0.1 \exp(-L), \\ m_{e\parallel} &= 0.12 + 0.16 \exp(-0.8L), \end{aligned} \quad (\text{B1})$$

that are shown on Fig. 7. However, we note that these

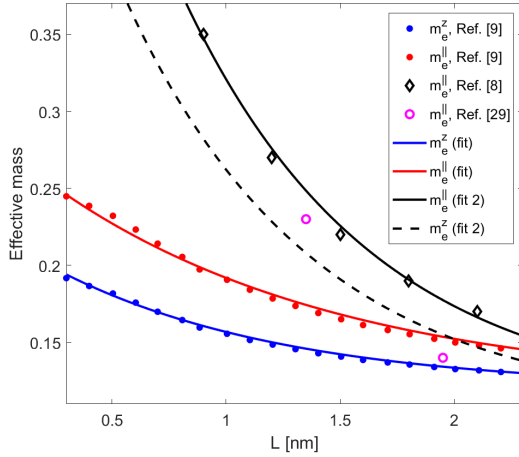


FIG. 7: Electron mass in CdSe nanoplatelet, fitted to the data from Refs. [8, 9, 29].

mass calculations are based on an assumption of constant hole masses ($m_{hzH} = 0.9$, $m_{h\parallel H} = 0.19$), which do not match other sources. On the other hand, in [8] an almost 40% larger mass m_{ez} is reported. It can be described by equation

$$m_{ez} = 0.11 + 0.7 \exp(-1.2L). \quad (\text{B2})$$

For the in-plane mass, we assume that the ratio $m_{ez}/m_{e\parallel}$ from [9] is maintained, resulting in a relation

$$m_{e\parallel} = 0.09 + 0.56 \exp(-1.2L). \quad (\text{B3})$$

Finally, we note that some of the difference in the masses originates from the fact that the calculations in [8] are performed for room temperature, while in [9] $T = 4.2$ K is used. Nevertheless, larger electron masses used in our calculations yield a better match to all spectra, including low-temperature ones.

For the heavy holes, we use a fit to the data from [8] for H1 hole, in the form

$$m_{hH}^{\parallel} = 0.6 \exp(-L) + 0.275 \quad (\text{B4})$$

The literature data for the mass m_{hH}^z are scarce; a constant value of $m_h^z = 0.9$ is proposed in [9], which is close

to the generally accepted bulk value [30]; however, for the best fit of binding energy, we propose the relation

$$m_{hH}^z = 2.1 \exp(-L) + 0.42. \quad (\text{B5})$$

The above fit approaches the above mentioned value of 0.9 in the limit of thick layer (1.5 nm \approx 5 monolayers), which is close to the limit of the applicability of our description. This fit not only results in the binding energy consistent with experimental measurements, but also allows us to estimate the light hole masses via Luttinger parameters and calculate the absorption spectrum containing both light- and heavy hole resonances consistent with experimental data.

The Luttinger parameters are given by

$$\begin{aligned} m_{hH}^z &= \frac{m_0}{\gamma_1 - 2\gamma_2}, \\ m_{hH}^{\parallel} &= \frac{m_0}{\gamma_1 + \gamma_2}, \\ m_{hL}^z &= \frac{m_0}{\gamma_1 + 2\gamma_2}, \\ m_{hL}^{\parallel} &= \frac{m_0}{\gamma_1 - \gamma_2}. \end{aligned} \quad (\text{B6})$$

With known masses m_{hH}^z , m_{hH}^{\parallel} , one can calculate γ_1 , γ_2 from the relations

$$\begin{aligned} \gamma_1 &= \frac{m_{h\parallel H} + 2m_{hzH}}{3m_{hzH}m_{h\parallel H}}, \\ \gamma_2 &= \frac{m_{hzH} - m_{h\parallel H}}{3m_{hzH}m_{h\parallel H}}. \end{aligned} \quad (\text{B7})$$

In the limit of a thin layer, the Luttinger parameters are consistent with those calculated in [31] for the case of a small quantum dot, which are $\gamma_1 = 1.66$, $\gamma_2 = 0.41$. With this, we can calculate light hole masses.

Next, we calculate the relevant reduced masses

$$\begin{aligned} \mu_{zH,L} &= \left(\frac{1}{m_e^z} + \frac{1}{m_{hH,L}^z} \right)^{-1}, \\ \mu_{\parallel H,L} &= \left(\frac{1}{m_e^{\parallel}} + \frac{1}{m_{hH,L}^{\parallel}} \right)^{-1} \end{aligned} \quad (\text{B8})$$

and the Rydberg energies

$$\begin{aligned} R_{ezH,L}^* &= \frac{\mu_{zH,L}}{\epsilon_1^2} 13.6 \text{ eV}, \\ R_{\parallel H,L}^* &= \frac{\mu_{\parallel H,L}}{\epsilon_1^2} 13.6 \text{ eV} \end{aligned} \quad (\text{B9})$$

We assume $\epsilon_1 = 6$, $\epsilon_2 = 2$ and

$$\gamma = \gamma_e + \gamma_h = 2 \frac{1}{4} \frac{\epsilon_1 - \epsilon_2}{\epsilon_1 + \epsilon_2} = \frac{1}{4} \quad (\text{B10})$$

In the calculations, we find the best fit to this data when using the electron and hole mass from [8], e.g. Eqs.

(B2,B3) and m_{hzH} given by Eq. (B5). For the in-plane mass, we use Eq. (B4), which is a fit to the data in [8]. With such a set of parameters, we obtain a binding energy that is consistent with both [8] and [9]. Importantly, such a set of parameters results in a calculated absorption spectrum that is in a good agreement with multiple experimental results [2, 9–12, 27]. The relevant parameters calculated for 3,4,5 monolayers are shown in Table II. We assume the monolayer thickness of 1/3 nm.

| Parameter | 3ML | 4ML | 5ML |
|----------------------------------|--------|--------|--------|
| L | 1 | 1.33 | 1.67 |
| m_{ez} | 0.2567 | 0.2015 | 0.1635 |
| $m_{e\parallel}$ | 0.3208 | 0.2519 | 0.2044 |
| m_{hzH} | 1.1925 | 0.9754 | 0.8153 |
| $m_{h\parallel H}$ | 0.4957 | 0.4337 | 0.3879 |
| m_{hzL} | 0.4149 | 0.3659 | 0.3302 |
| $m_{h\parallel L}$ | 0.8121 | 0.6887 | 0.5963 |
| μ_{zH} | 0.2112 | 0.1670 | 0.1362 |
| $\mu_{\parallel H}$ | 0.1948 | 0.1593 | 0.1338 |
| μ_{zL} | 0.1586 | 0.1300 | 0.1094 |
| $\mu_{\parallel L}$ | 0.2300 | 0.1844 | 0.1522 |
| $p_H = \mu_{\parallel H}/m_{ez}$ | 0.7589 | 0.7907 | 0.8165 |
| $p_L = \mu_{\parallel L}/m_{ez}$ | 0.8960 | 0.9152 | 0.9298 |
| $R_{\parallel H}^*$ | 73.58 | 60.20 | 51.28 |
| $R_{\parallel L}^*$ | 86.88 | 69.67 | 58.39 |
| γ_1 | 1.6243 | 1.8789 | 2.1062 |
| γ_2 | 0.3929 | 0.4269 | 0.4488 |

TABLE II: Masses, reduced masses, Rydberg energies, Luttinger parameters

- [1] A. Ekimov, A. Onushchenko, Quantum size effect in 3-dimensional microscopic semiconductor crystals, *JETP Lett.* **34**, 345-349 (1981).
- [2] J. Yu, R. Chen, Optical properties and applications of two-dimensional CdSe nanoplatelets, *InfoMat* **2**, 5, 905-927 (2020).
- [3] A. Dutta, A. Medda, and A. Patra, Recent Advances and Perspectives on Colloidal Semiconductor Nanoplatelets for Optoelectronic Applications, *The Journal of Physical Chemistry C* **125** (1), 20-30 (2021).
- [4] Murray CB, Norris DJ, Bawendi MG. Synthesis and characterization of nearly monodisperse CdE (E = S, Se, Te) semiconductor nanocrystallites. *J Am Chem Soc.* 115, 8706-8715 (1993).
- [5] Joo J, Son JS, Kwon SG, Yu JH, Hyeon T. Low-temperature solution-phase synthesis of quantum well structured CdSe nanoribbons. *J Am Chem Soc.*,128, 5632-5633 (2006).
- [6] M. D. Tessier, C. Javaux, I. Maksimovic, V. Lorientte, B. Dubertret, Spectroscopy of single CdSe nanoplatelets, *ACS Nano* **6**(8), 6751-8 (2012).
- [7] B. T. Diroll and R. D. Schaller, Reexamination of the Giant Oscillator Strength Effect in CdSe Nanoplatelets, *J. Phys. Chem. C*, 127, 9, 4601-4608 (2023).
- [8] R. Benchamekh, N. A. Gippius, J. Even, M. O. Nestoklon, J.M. Jancu, S. Ithurria, B. Dubertret, A. L. Efros, and P. Voisin, Tight-binding calculations of image-charge effects in colloidal nanoscale platelets of CdSe, *Phys. Rev. B* **89**, 035307 (2014).
- [9] E. V. Shornikova, D. R. Yakovlev, N. A. Gippius, G. Qiang, B. Dunertet, A. H. Khan, A. Di Giacomo, I. Moreels, and M. Bayer, Exciton binding energy in CdSe nanoplatelets measured by one- and two-photon absorption, *Nano Lett.* **21**, 10525 (2021).
- [10] S. J. Zelewski, K. C. Nawrot, A. Zak, M. Gladysiewicz, M. Nyk, and R. Kudrawiec, Exciton Binding Energy of Two-Dimensional Highly Luminescent Colloidal Nanostructures Determined from Combined Optical and Photoacoustic Spectroscopies, *J. Phys. Chem. Lett.***10**, 3459-3464 (2019).
- [11] D. A. Baghdasaryan, V. A. Harutyunyan, D. B. Hayrapetyan, E. M. Kazaryan, S. Baskoutas, and H. A. Sarkisyan, Exciton States and Optical Absorption in CdSe and PbSN Nanoplatelets, *Nanomaterials* **12**, 3690 (2022).
- [12] A. Brumberg, S. M. Harvey, J. P. Philbin, B., T. Diroll, Byeongdu Lee, S. A. Crooker, M. R. Wasielewski, E. Rabani, and R. D. Schaller, Determination of the In-Plane Exciton Radius in 2D CdSe Nanoplatelets via Magneto-optical Spectroscopy, *ACS Nano* 2019, 13, 8, 8589-8596, <https://doi.org/10.1021/acsnano.9b02008>.
- [13] G. Czajkowski, F. Bassani, and L. Silvestri, Excitonic optical properties of nanostructures: real density matrix approach, *Riv. Nuovo Cimento* **26**, 1 (2003). DOI 10.1393/ncr/i2003-10002-2.
- [14] T. Kazimierzczuk, D. Fröhlich, S. Scheel, H. Stolz, and M. Bayer, Giant Rydberg excitons in the copper oxide Cu₂O, *Nature* **514**, 344 (2014).
- [15] M. Aßmann and M. Bayer, Semiconductor Rydberg Physics, *Advanced Quantum technologies*, 1900134 (2020). DOI: 10.1002/qute.201900134.
- [16] D. Ziemkiewicz, G. Czajkowski, and S. Zielińska-Raczyńska, Optical properties of Rydberg excitons in Cu₂O-based superlattices, *Phys. Rev. B.* **109**, 085309 (2024), DOI: 10.1103/PhysRevB.109.085309.
- [17] C. Morin, J. Tignon, J. Mangeney, S. Dhillon, G.

- Czajkowski, K. Karpiński, S. Zielińska-Raczyńska, D. Ziemkiewicz, and T. Boulier, Self-Kerr effect across the yellow Cu_2O Rydberg series, *Phys. Rev. Lett.* **129**, 137401 (2022). DOI:10.1103/PhysRevLett.129.137401.
- [18] W. Huhn and A. Stahl, Self-consistent field theory applied to semiconductor band edge, *Phys. Status Solidi B* **124**, 167 (1984).
- [19] A. Stahl, Electrodynamics of the band-edge in a direct gap semiconductor, *Solid State Commun.* **49**, 91-93 (1984).
- [20] A. Stahl and I. Balslev, *Electrodynamics of the Semiconductor Band Edge* (Springer-Verlag, Berlin-Heidelberg-New York, 1987).
- [21] L. D. Landau and E. M. Lifshitz, *Electrodynamics of Continuous Media*, 2nd Ed. by E. M. Lifshitz and L. P. Pitaevskii (Pergamon Press, Oxford, 1984).
- [22] S. Caicedo-Davila, P. Caprioglio, F. Lehmann, S. Levenco, M. Stolterfoht, D. Neher, L. Kronik, and Daniel Abou-Ras, Effects of Quantum and Dielectric Confinement on the Emission of Cs-Pb-Br Composites, *Adv. Func. Mater.* **33**, 2305240 (2023).
- [23] D. Ziemkiewicz, K. Karpiński, G. Czajkowski, and S. Zielińska-Raczyńska, Excitons in Cu_2O : From quantum dots to bulk crystals and additional boundary conditions for Rydberg exciton-polaritons, *Phys. Rev. B* **101**, 205202 (2020).
- [24] B. Ji, E. Rabani, A. Efros, R. Vaxenburg, O. Ashkenazi, D. Azulay, U. Banin, O. Millo, Dielectric confinement and excitonic effects in two-dimensional nanoplatelets. *ACS Nano* **14**, 8257-8265 (2020).
- [25] E. V. Shornikova, L. Biadala, D. R. Yakovlev, V. F. Sapaga, Y. G. Kusrayev, A. A. Mitioglu, M. V. Ballottin, P. C. M. Christianen, V. V. Belykh, M. V. Kochiev, N. N. Sibeldin, A. A. Golovatenko, A. V. Rodina, N. A. Gippius, A. Kuntzmann, Y. Jiang, M. Nasilowski, B. Dubertret, and M. Bayer, Addressing the exciton fine structure in colloidal nanocrystals: the case of CdSe nanoplatelets, *Nanoscale* **10**, 646-656 (2018).
- [26] M. Abramowitz and I. Stegun, *Handbook of Mathematical Functions* (Dover Publications, New York, 1965).
- [27] A.M. Smirnova, V.N. Mantsevich, D.S. Smirnov, A.D. Golinskaya, M.V. Kozlova, B.M. Saidzhonov, V.S. Dneprovskii, R.B. Vasiliev, Heavy-hole and light-hole excitons in nonlinear absorption spectra of colloidal nanoplatelets, *Solid State Commun.* **299**, 113651 (2019).
- [28] P. Bai, An Hu, Yunzhou Deng, Zhenyu Tang, Wenjin Yu, Yanlei Hao, Shuang Yang, Yunke Zhu, Lixin Xiao, Yizheng Jin, ang Yunan Gao, CdSe/CdSeS Nanoplatelet Light-Emitting Diodes with Ultrapure Green Color and High External Quantum Efficiency, *The Journal of Physical Chemistry Letters*, 9051-9057 (2022).
- [29] H. Yeo, J. S. Lee, M. E. Khan, H. S. Kim, D. Y. Jeon, and Y.-H Kim, Approximation for the improved description of quantum nanostructures, *Journ. Phys. Mater.* **3**, 034012 (2020). <https://doi.org/10.1088/2515-7639/ab9b61> *Journal of Physics: Materials*.
- [30] A. I. Kashuba, B. Andriyevsky, H. A. Ilchuk, R. Y. Petrus, T. S. Malyi, I. V. Semkiv, Electronic structure and elastic properties of $\text{Cd}_{16}\text{Se}_{15}\text{Te}$ solid state solution: first principles study, *Condensed Matter Physics* **24**, 2, 23702, 1-10 (2021).
- [31] U. E. H. Laheld and G. T. Einevoll, Excitons in CdSe quantum dots, *Phys. Rev. B* **55**, 5184 (1997).